PHILOSOPHICAL TRANSACTIONS A

Phil. Trans. R. Soc. A.
doi:10.1098/not yet assigned

Ice Giant Magnetospheres

Carol Paty[1,*], Chris S. Arridge[2], Ian J. Cohen[3], Gina A. DiBraccio[4], Robert W. Ebert[5,6], Abigail M. Rymer[3]

[1]*Department of Earth Sciences, University of Oregon, 100 Cascade Hall, Eugene, OR 97403-1272, USA, ID: 0000-0001-8362-9880*

[2]*Department of Physics, Lancaster University, Bailrigg, Lancaster, LA1 4YW, UK, ID: 0000-0002-0431-6526*

[3]*Johns Hopkins Applied Physics Laboratory, 11000 Johns Hopkins Road, Laurel, MD, 20723-6005, USA, ID IJC: 0000-0002-9163-6009 AMR ID: 0000-0002-4879-0748*

[4]*NASA Goddard Space Flight Center, Greenbelt, MD 20771 USA, ID: 0000-0002-2778-4998*

[5]*Southwest Research Institute, San Antonio, TX, 78228-0510, USA, ID: 0000-0002-2504-4320*

[6]*Department of Physics and Astronomy, University of Texas at San Antonio, TX, USA 78249-0600*

Keywords: Neptune, Uranus, Magnetosphere, Radiation Belts, Plasma

Summary

The ice giant planets provide some of the most interesting natural laboratories for studying the influence of large obliquities, rapid rotation, highly-asymmetric magnetic fields, and wide-ranging Alfvénic and sonic Mach numbers on magnetospheric processes. The geometries of the solar wind-magnetosphere interaction at the ice giants vary dramatically on diurnal timescales due to the large tilt of the magnetic axis relative to each planet's rotational axis and the apparent off-centered nature of the magnetic field. There is also a seasonal effect on this interaction geometry due to the large obliquity of each planet (especially Uranus). With *in situ* observations at Uranus and Neptune limited to a single encounter by the Voyager 2 spacecraft, a growing number of analytical and numerical models have been put forward to characterize these unique magnetospheres and test hypotheses related to the magnetic structures and the distribution of plasma observed. Yet many questions regarding magnetospheric structure and dynamics, magnetospheric coupling to the ionosphere and atmosphere, and potential interactions with orbiting satellites remain unanswered. Continuing to study and explore ice giant magnetospheres is important for comparative planetology as they represent critical benchmarks on a broad spectrum of planetary magnetospheric interactions, and provide insight beyond the scope of our own solar system with implications for exoplanet magnetospheres and magnetic reversals.

*Author for correspondence (cpaty@uoregon.edu).
†Present address:
Department of Earth Sciences, University of Oregon,
100 Cascade Hall, Eugene, OR 97403-1272, USA

Main Text

1. Introduction

The magnetospheres of Uranus and Neptune are unlike those of their gas giant neighbors, and far from the canonical template drawn from the generations of spacecraft orbiting and characterizing Earth's near-space environment. Each of these ice giant planets possess a highly tilted dipolar magnetic moment with a strong quadrupole moment [1], which combined with obliquity create magnetospheres rife with asymmetries and with strong diurnal and seasonal variability. From the constantly shifting regions of reconnection across the magnetopause on daily and seasonal scales [2,3,4,5,6], to their helically twisted magnetotails and curved current sheets [7,8,9,10,11], the ice giant magnetospheres represent critical departures from the standard model and implore further study with the questions they raise.

Their distant location from the Sun (19.8 and 30.0 AU respectively) also leads to a significant difference in the local solar wind characteristics at Uranus and Neptune as compared to that experienced at Earth. The local flow regime governs the type of interaction across the planetary bow shock and magnetopause, where energy transfer from the solar wind to the magnetospheric plasma population occurs. A transition from solar wind-driven global magnetic reconnection to a more viscous-like interaction where the magnetopause boundary enables the growth of the Kelvin-Helmholtz instability is likely in the outer solar system [12], and has implications for inner magnetospheric dynamics at the ice giants. The cusp entry of the solar wind is also quite different at the ice giants when compared to the terrestrial case. At both Uranus and Neptune, the combination of their obliquity with the large tilt of their primary dipole, and the strong contribution from higher-order terms of the magnetic field expansion, create periods modulated by rotation and season when the cusp can point into or nearly into the solar wind.

Given the limited observational data, it can be useful to characterize the ice giant magnetospheres in terms of other well-studied planets in the solar system [e.g. 13]. Unlike Earth's magnetosphere, which is dynamically driven by the solar wind [e.g. 14, and references therein], the magnetospheres of Uranus and Neptune may only weakly couple to the solar wind. Jupiter and Saturn have volcanic (and cryovolcanic) moons and rings which provide strong plasma sources to the inner magnetosphere [15,16]. Due to their rapidly rotating magnetospheres, that plasma is accelerated to nearly corotational speeds and radially transported via plasma injection events at Jupiter [17, 18, 19] and at Saturn [20,21,22].

The thick exosphere and ionosphere of Triton, Neptune's largest satellite, likely provides a significant source of mass loading to Neptune's outer magnetosphere in the form ion escape and neutral loss that goes on to be ionized [23]. Although its orbital location of 14 R_N places it well inside the magnetopause (at 23-26 R_N), there were no observations of injection events during Voyager 2's encounter with Neptune's magnetosphere [24]. Uranus' magnetosphere contained very little plasma, but injection-like events were observed [25] and were likely driven by reconnection in the magnetotail. The presence of these injection events may help to explain the observed radiation belt energy spectrum and supports the recent identification of a plasmoid during the Voyager 2 traverse of Uranus' magnetotail [26].

Both Uranus and Neptune possess radiation belts observed by the Voyager 2 spacecraft [25,27]. These are nominally populated by energetic charged particles from the 100 keV into the MeV energy range. Unexpectedly, Uranus' electron radiation belts were observed to be as intense as those of Earth and Jupiter up to 1 MeV, while Neptune's radiation belts were the most quiescent yet observed in the solar system and host to the lowest proton radiation belt fluxes [28, 29]. One contributing factor structuring the radiation belts is the local magnetic field strength and configuration. If field lines are very dipolar and the solar wind electric field penetration is limited (e.g., Jupiter), then particles can remain quasi-stably trapped and strong fluxes can accumulate. One might conclude that Saturn's dipolar field would similarly trap intense radiation belts, however, the presence of Saturn's high-density neutral cloud [30,31] reduces the energetic ion population through processes like charge exchange [32]. The trapped energetic electrons at Saturn are affected by frequent collisions with neutrals (loss of energy), ring particles, and icy moons (loss of particles) [33, 29].

The magnetospheres of our solar system's ice giants represent a different class of magnetosphere, perhaps most associable with the configuration presumed during Earth's magnetic reversal [34], and perhaps to those found in exoplanet populations. The Voyager 2 mission shed the first light on these intriguing planetary magnetospheres over 30 years ago, and remains the sole source of *in situ* measurements at both Uranus and Neptune, raising many more questions with the brief but revealing observations collected. In the following, we detail the state of our current knowledge of ice giant magnetospheres, stemming from the Voyager 2 encounters and expanded by modelling and remote observations, and conclude with some of the evolving questions that motivate future exploration of these understudied worlds.

2. Asymmetric magnetospheric geometry

Most planets in the solar system have their magnetic dipoles nearly aligned with their spin axes, both of which are approximately (within a few tens of degrees) perpendicular to the solar wind flow direction. In contrast, Uranus and Neptune have highly inclined magnetic dipoles, which, in combination with their respective obliquities, provide periods where the angle between their magnetic dipole axes and the solar wind approaches 0° or 180° - the dipole axes alternate between pointing towards or away from the Sun. This instantaneous angle between the magnetic dipole and the planet-Sun vector is referred to as the solar wind attack angle [35,36], a characteristic that impacts many magnetospheric processes and is predominantly controlled by two factors: a) rotation of the planet with a tilted dipole (diurnal variation), and b) seasons which change the angle of the spin axis to the solar wind. Thus, the behavior of the attack angle can be thought of as a diurnal modulation about a slower seasonal modulation (e.g., Figure 6 in Lepping [35]).

Like other magnetized planets in the solar system, the internal magnetic fields of Uranus and Neptune can, to first order, be adequately modelled as offset-tilted (eccentric) dipoles; however, this is where the commonality ends. Most planetary dipoles have a tilt of around 10° or less relative to their axes of rotation, whereas Uranus and Neptune are significantly tilted with dipole colatitudes of 60.0° and 46.8°, respectively [7,37,1]. The dipole offsets of Saturn and Mercury are essentially axial shifts along the rotation axis whereas Jupiter has a modest shift off the rotation axis in the equatorial plane [38,39]. The dipole offsets for Uranus and Neptune are three-to-five times larger, with Neptune's dipole exhibiting a significant offset in three

dimensions, whereas Uranus' has an axial shift. These significant offsets are due to the relatively large contribution of the quadrupole magnetic moment to the total field, and are readily visible in Figure 1 which shows a sketch of the orientations of Uranus and Neptune at the times of the Voyager 2 flybys in 1986 and 1989, respectively.

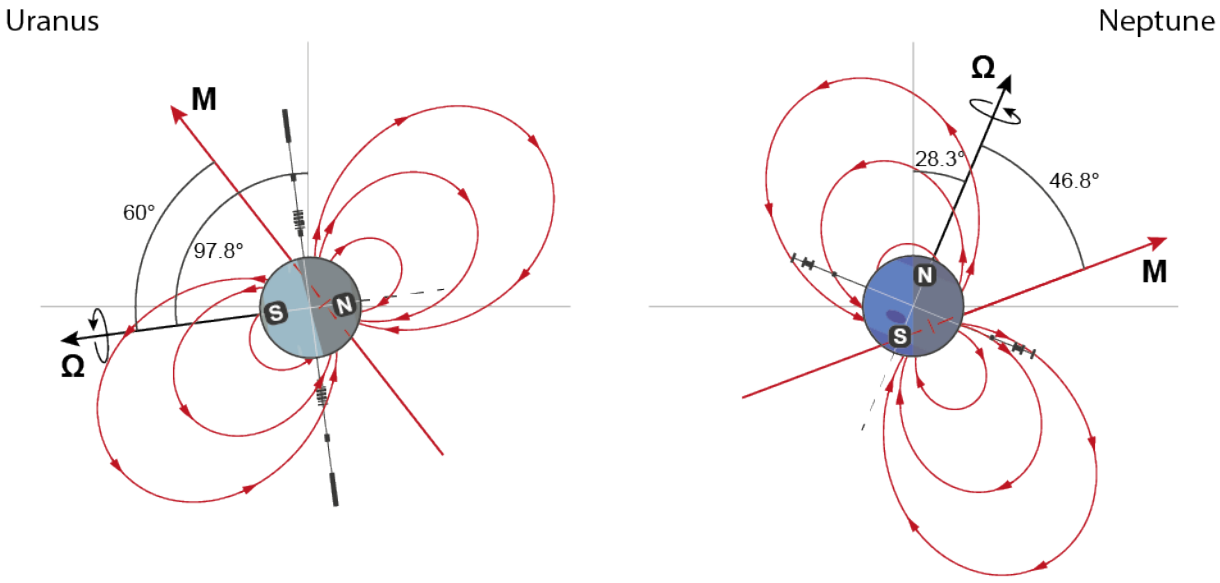

*Figure 1: Sketch of the offset tilted dipole field lines (red), dipole axis **M** (red), rotation axis **Ω** (black) for Uranus (left) and Neptune (right). Note that the north and south poles are reversed in this view for the left panel as we draw this schematic using the IAU definition for Uranus' poles. The white lines mapped over the planets illustrate the rotational axis and rotational equator, and the red dashed line is the magnetic axis, hashed at the off-centered location of the magnetic moment. The ring plane is identified by the schematic representation of the discrete and diffuse rings in black.*

The obliquity, shown by the tilt angle of the rotation axis **Ω** in Figure 1, of Neptune is not distinguished amongst the planets but Uranus's obliquity is very large and results in periods when the satellite orbital plane becomes perpendicular to the planet-Sun line (for example at the epoch of the Voyager 2 flyby). In spite of the somewhat similar dipole tilt angles, this difference in obliquities results in fundamentally different behavior. Near solstice at the time of the Voyager 2 encounter, Uranus' dipole was almost perpendicular to the solar wind, with an average attack angle of 60°, and so could be thought of as similar to Earth's magnetosphere, but with diurnal rotation about the planet-Sun line twisting up the magnetotail. Neptune was encountered by Voyager 2 when the attack angle varied between around 60° and 170° (i.e., between perpendicular and pole-on to the solar wind). Uranus encounters a similar configuration near equinox. When Neptune approaches equinox the angle of attack is centered around a perpendicular configuration, varying up to 45° towards or away from the Sun [e.g., 36,40].

We must add another symmetry surface to the rotational and magnetic equators: the centrifugal equator. Plasma in the magnetosphere is affected by the field-aligned component of the centrifugal force and its

equilibrium location is the centrifugal equator. Radiation belt particles are sufficiently energetic that they are not significantly affected, but for cold particles, whose thermal energy is small compared to the rotational kinetic energy, the centrifugal equator lies at 16.9° and 22.7° from the magnetic equator at Uranus and Neptune, respectively [36,41]. It is also important to point out that Triton is thought to be an important source of neutrals at Neptune [e.g., 42] and is in a highly inclined retrograde orbit, adding a layer of complexity to the interaction with the centrifugal equator. The magnetospheres of Uranus and Neptune are truly three-dimensional and two-dimensional cuts are of limiting value, particularly away from limiting cases [36]. Hence, 3D visualization tools (for example, [43]) are necessary to understand the resulting geometry.

Closer to the planet, higher-degree multipoles are required to adequately model the internal planetary field; these are obtained from a spherical harmonic expansion of the magnetic scalar potential. In this representation the offset of the dipole can be related to the quadrupole (n=2) terms of the expansion [e.g., 44]. The internal planetary fields of Uranus and Neptune are unique in the solar system for their general multipolar structure (see for example, *Soderlund et al.* this volume, and *Stanley and Bloxham* [45]). The offset and tilted dipole model naturally results in large excursions in magnetic latitude (or equivalently, large excursions in L-shell [46]) experienced by a natural satellite or spacecraft as the planet rotates, and higher degree multipoles produce drift shell splitting. In combination these factors are important for understanding energetic particle distributions. In a centered, dipole magnetic field geometry the location of mirror points can be identified based on pitch angle and field strength at some point on the field lines. However, multipolar fields break this simple picture. Indeed, along some field lines there is not a minimum in field strength and particles on these field lines will never mirror and are lost to the planet's atmosphere in less than a single bounce period [47].

Convection is also strongly affected by asymmetry; in the general case, where the spin axis, solar wind vector, and magnetic dipole vector are all non-orthogonal, there is no frame in which convection can be assumed to be time-independent [48]. Luckily, there are times where convection can be examined in limiting cases, for example when the dipole is perpendicular to both the rotation axis and the solar wind (e.g., Uranus at Voyager 2) or the spin axis perpendicular to the solar wind. Self-consistent calculations for plasma convection have been carried out for Uranus at solstice and show sunward convection with a shielded region inside 5 R_U (similar to that observed by Voyager 2). Higher-degree multipoles have a considerable effect on this convection, both distorting streamlines and changing the shape of the shielded region [49].

The subsolar magnetopause at Uranus and Neptune was found to be 18 R_U and 23-26 R_N, respectively [50] and the bow shock at 22.5 R_U and 34.9 R_N, respectively [7,37]. As the solar wind attack angle varies, the magnetopause location might be expected to vary diurnally (in three-dimensions) as different colatitudes are involved in local pressure balance at the magnetopause, pushing out the magnetopause or permitting it to move closer to the planet. While the encounter geometry of Voyager 2 made it challenging to observe such magnetopause variability at Uranus, these effects were inferred from modulations (38-43 R_N to 38.5 to 34.5 R_N) in Neptune's bow shock stand-off distance [51]. At Neptune, the trajectory of Voyager 2 also took the spacecraft through the cusp and mantle as the dipole was pole-on during the inbound leg on the dayside [52].

3. Magnetotail structure and dynamics

A magnetotail forms as a result of the solar wind's interaction with a planetary magnetic field, elongating the fields behind the planet to create a stretched magnetic tail. The dipolar magnetic structure at Uranus and Neptune leads to the formation of two distinct magnetotail lobes, one directed toward the planet and the other directed away, separated by a cross-tail current sheet. This initial structure is similar to that of the intrinsic magnetotails of Earth, Jupiter, and Saturn; however, the highly-inclined rotation and magnetic axes distort the magnetotail structure.

Prior to the arrival of Voyager 2 at Uranus, hydrogen Ly-α emission observations led Siscoe [53] and later Hill et al. [54] to predict that the combination of planetary rotation and solar wind interactions should result in a helical twist of magnetotail. Several years later, Ness et al. [7] and Behannon et al. [8] confirmed that the magnetotail, constituted by two bipolar lobes, rotates about the sun-planetary line on the same timescale of a ~17 h Uranus day (Figure 2a). These first *in situ* measurements at Uranus constrained the tail radius to be ~42 R_U at the time of the flyby, with a helically-twisted structure that is slightly less inclined than earlier predictions (Figure 2b). More recently, modeling work has supported these observations and enhanced our understanding of the magnetotail structuring by investigating the magnetotail twist (Figure 2c) during Uranus solstice (as experienced by Voyager 2) [10], the variations in tail asymmetries as a function of diurnal and seasonal effects [5], and the general effects of planetary rotation (modeled at 10 times the actual rotation rate for computational tractability) on magnetotail morphology and changes in the tail twist angle [11]. Cowley [55] considered the structure of Uranus' magnetotail during equinox, and proposed that the formation of an elongated bipolar magnetotail could be suppressed by rotational winding of open magnetic flux tubes over the dayside magnetopause. While this prediction posed a potential explanation for the weak auroral signatures observed by Hubble Space Telescope at equinox [56], plasma dynamic simulations of Uranus' magnetosphere in equinox configuration did not demonstrate this effect [5]. For Neptune, the trajectory of Voyager 2 combined with the planet's obliquity led to observations in a single lobe of the magnetotail and plasma sheet, without crossing the current sheet [37]. Recent modeling efforts have demonstrated that Neptune's tail is likely a dual-lobe structure, separated by a single current sheet, with a twisted configuration due to the planetary rotation (Mejnertsen et al., [4] and references therein).

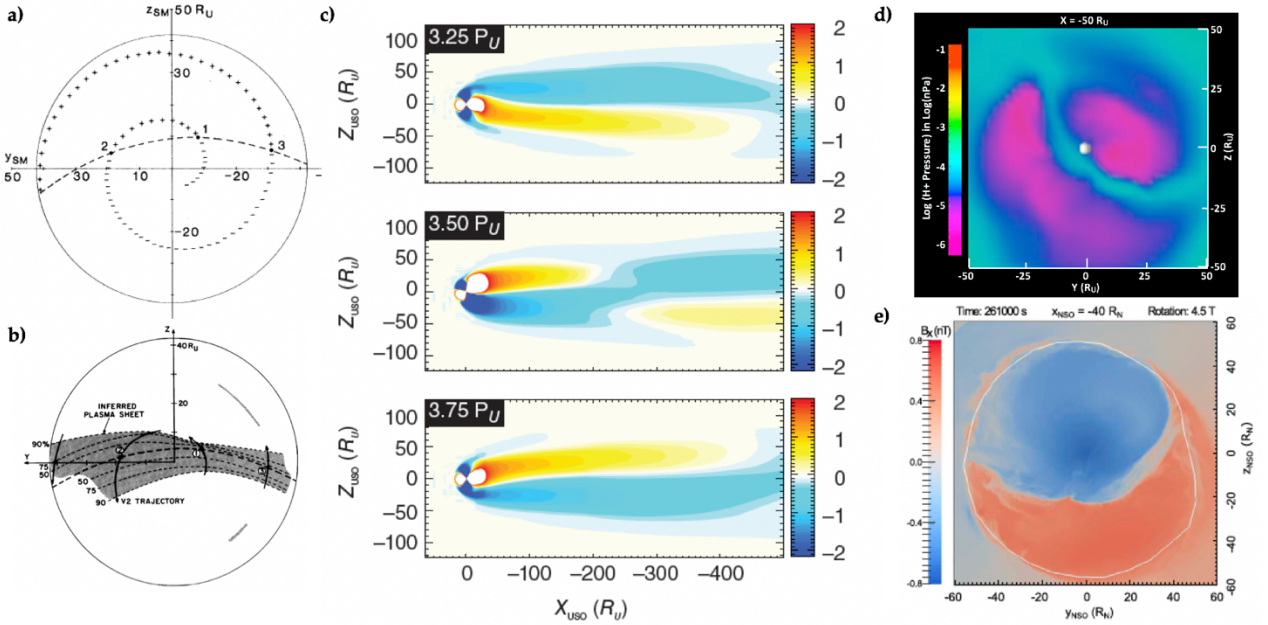

Figure 2: Uranus' magnetotail as observed by Voyager 2's outbound trajectory where it (a) passed through the alternating polarity of the lobes (from Figure 5 in Ness et al., [7]). Panel (b) shows the inferred curved plasma sheet geometry (from Figure 5, Behannon et al. [8]), and panel (c) the model prediction of the twisted helical tail (after Toth et al. [10] and Arridge, [39]). Panel (d) shows the modelled rotation of the curved plasma sheet in a slice looking down-tail during Uranus solstice conditions (from Cao and Paty [5]). The last panel (e) is a visualization of the modelled current sheet of Neptune looking down-tail for the pole-on configuration (from Mejnertsen et a. [4]).

During the flybys of Uranus and Neptune, Voyager 2 spent a majority of the transit time within each planetary magnetotail. Behannon et al. [8] performed an in-depth analysis on Uranus' magnetotail and determined that the plasma sheet had a thickness ranging from ~10 R_U to greater than 25 R_U. Within the plasma sheet, the cross-tail current sheet is likely asymmetric and curved as a result of a lag with the planetary rotation that causes the tail to twist. This finding was further supported by modeling efforts, which demonstrated that the curvature of the current sheet varied with changes in the dipole tilt over a planetary rotation [57,9]. The results presented by Cao and Paty [5] also concluded that the curved and twisted plasma sheet structure is related to a combination of the offset, tilted planetary dipole field along with the solar wind-planetary interaction (Figure 2d). For the case of Neptune, knowledge of magnetotail characteristics are still limited due to the Voyager 2 trajectory [35], but modeling results prove to be a powerful tool in combining our knowledge from Uranus and applying this to Neptune. Mejnertsen et al. [4] investigated the two proposed magnetosphere configurations during the Voyager 2 flyby and their magnetohydrodynamic model indicated that the tail current sheet always closes on the magnetopause (Figure 2e), a prediction in contrast to that posed by Voigt and Ness [58] where the tail current was modelled to close on itself during pole-on configuration.

By revisiting the Voyager 2 flyby data more than three decades later, DiBraccio and Gershman [26] reported the detection of a magnetic plasmoid within the magnetotail of Uranus. The plasmoid, a magnetic bubble filled with plasma likely of planetary origin, was travelling downtail and away from the planet. The observation of a plasmoid within Uranus' magnetotail indicates that magnetic reconnection occurred within the tail current sheet to detach from the planetary field. The structure of the plasmoid provides clues to whether the convection of plasma within the magnetosphere of Uranus is externally driven by the solar wind, like Earth, or internally driven, like Jupiter and Saturn. This particular plasmoid structure was reminiscent of those identified at the gas giants [see 59,60,61,62], pointing to internal driving; however, the plasmoid signature was succeeded by a post-plasmoid plasma sheet, indicating that solar wind-driven reconnection was likely occurring between the magnetotail lobes [63]. It is hypothesized that these plasmoids are common within the magnetotail of Uranus and may occur on timescales of ~17 h [60] or more often. Although plasmoids probably exist at Neptune as well, they were not detected during the Voyager 2 flyby, likely due to the fact that the spacecraft trajectory did not cross the tail current sheet.

4. Solar Wind in the Outer Solar System

The interaction between the solar wind and a planetary magnetosphere is often parameterized in terms of the Alfvénic Mach number (M_A), which is a dimensionless comparison between the solar wind's dynamic and magnetic pressures. In the inner heliosphere, observations of lower M_A values in the solar wind, and therefore low plasma β (the ratio of thermal pressure to magnetic pressure) in the magnetosheath, have been attributed to the continuous solar wind-driven dynamics. In the outer heliosphere, however, M_A values are typically higher as a result of changes in solar wind density and magnetic field magnitude with distance from the sun, following the Parker model [*65*], and solar wind forcing is considerably weaker. To determine the degree to which external forces versus internal forces play a dominant role in a given magnetosphere, *Swisdak et al.* [66,67] established a relationship between the change in magnetosheath β across a planetary magnetopause with the magnetic shear between the interplanetary magnetic field (IMF) and planetary field. Using this relation, it is possible to theorize whether magnetic reconnection is possible or suppressed along a magnetopause for a set of conditions. This method has been implemented for the solar wind-driven magnetospheres of Mercury [68,69] and Earth [e.g., 70,71], as well as the internally-driven systems of Jupiter [72, 73, 74] and Saturn [75,76]. With minimal data to determine whether solar wind and planetary conditions are favorable for externally-driven convection at the ice giants, the Swisdak relation has been implemented using an analytical assessment for both Uranus [2] and Neptune [3]. *Masters* [2] predicted that at Uranus during solstice, the conditions across the magnetopause were more permissive of magnetic reconnection than during equinox, though both seasons were rotationally modulated depending on the orientation of the solar wind and the evolving magnetic shear. Similar analysis at Neptune indicated that the fraction of the magnetopause surface where reconnection was possible was reduced compared to Uranus during solstice, though still rotationally modulated [3]. The equinox case for Neptune heavily favored reconnection during the pole-on configuration when the magnetic shear with the IMF was maximized. The daily opening and closing of the magnetosphere indicated by these analytical models, were mirrored in the 3D dynamic models of Cao

and Paty [5] (Uranus) and Mejnertsen et al. [4] (Neptune) which both indicated strong diurnal modulation of reconnection.

It is important to note that beyond the assessment of plasma β and magnetic shear in determining the potential for reconnection across the magnetopause, it is useful to examine the relative likelihood of magnetic reconnection versus a more viscous interaction [12]. This balance between the strength of the reconnection electric field and the growth of the Kelvin-Helmholtz instability is governed by local solar wind conditions, specifically the solar wind Alfvén speed and associated M_A. Typical M_A values at Earth are ~5-8 and increase to >10 in the outer heliosphere (> 5 AU) [77,40,6]. *In situ* observations of solar wind conditions at the time of the Voyager 2 encounter of Uranus demonstrated a high upstream M_A ~23 [78]. However, the Voyager 2 Neptune flyby measured a much lower M_A value of ~9 [79], which is close to inner-heliospheric conditions. The latter case suggests that M_A does not simply increase with increasing distance from the Sun, but rather, that there is a high degree of variability in this parameter throughout the outer heliosphere. To determine the spatial and temporal trends of M_A throughout the heliosphere, *Gershman and DiBraccio* [6] analyze more than 30 years of *in situ* plasma and fields data spanning from 0.3 to 75 AU. The results of this investigation demonstrated that average trends in M_A follow expectations based on the Parker model of changes in solar wind and IMF properties with distance from the Sun; however, actual values of M_A are significantly modulated as a function of solar activity. More specifically, magnetic pressure increases during solar maximum while dynamic pressure remains constant, generating lower M_A values overall. During these periods of solar maximum, M_A regularly falls below ~8 upstream of the giant planets in the outer heliosphere. For the case of the Voyager 2 encounters at the ice giants, the sun was in a state of decreased activity during the 1986 Uranus flyby but had begun to increase in activity levels during the 1989 Neptune encounter.

The observational evidence that M_A is affected by changes in solar cycle has great implications for solar wind-planetary coupling at the ice giants. That is, during times of solar maximum when M_A can reach inner heliospheric values at the ice giants, solar wind coupling through magnetic reconnection may occur more often than once predicted. *Gershman and DiBraccio* [6] explored this possibility by utilizing the solar wind measurements in the outer heliosphere and applying the Swisdak relation under planetary magnetic field conditions representative of Uranus and Neptune. The results demonstrated that the planetary geometries of the ice giants, when considering both the rotation and magnetic axes tilts, creates conditions for frequent magnetopause reconnection. This is because the tilts introduce scenarios with greater variability in magnetic shear between the planetary field and the IMF compared to the neighboring gas giants.

Following the Voyager 2 flyby of Uranus, *Vasyliunas* [48] theorized that the combination of weaker plasma sources internal to the magnetospheres of Uranus and Neptune, combined with the tilted rotation and dipole geometries, likely enables increased solar wind-driving during epochs where corotation and convection are decoupled. The added understanding that upstream M_A varies as a function of solar cycle and can reach inner heliospheric values encouraging a higher level of solar wind-magnetosphere coupling, suggests that it is important to consider changes in both internal and external conditions. The combination of solar maximum and planetary seasons that create high shears between the IMF and planetary fields generate conditions that are favorable for magnetopause reconnection to occur [6]. Therefore, the ice giant magnetospheres may be

more solar wind driven than initially concluded from propagating nominal solar wind conditions in the inner solar system to 10s of AU [12].

5. Magnetospheric Plasma Populations

The plasma and energetic particle distributions in the magnetospheres of Uranus and Neptune were characterized by *in situ* measurements from the Plasma Science Experiment (PLS) [80] and Low-energy Charged Particle (LECP) instrument [81] on Voyager 2.

At Uranus, the plasma was concluded to be primarily composed of protons and electrons based on consistency of the total ion plasma and waves measurements with a proton-dominated plasma under corotation [82,83]; very little *in situ* information is known about ion composition of Uranus' magnetosphere. These assumed protons contained a warm population (T ~ 10 – 30 eV, N_{peak} ~ 2 cm^{-3}) characterized by a Maxwellian-core that was subsonic and was observed throughout the magnetosphere while intermediate (T ~ 20 – 200 eV, N_{peak} ~ 1.0 cm^{-3}) and hot (T ~ 1 keV, n_{peak} ~ 0.5 cm^{-3}) non-thermal populations were confined to regions beyond L-shell ~ 5 due to shielding from the convective electric field [82,83,84]. Current estimates place the plasma source rate at ~0.02 kg/s [50], several orders of magnitude below what is observed at Jupiter [e.g., 85] and Saturn [e.g., 86,87] and even an order of magnitude below the estimated plasma source rate for Neptune [e.g., 88]. Only an upper limit of 0.01 cm^{-3} was placed on the heavy ion density below 6 keV/q [78] and the mass composition of the ions was only more strongly constrained at energies > 500 keV/nucleon [25], but was found to be composed primarily of protons, with H_2^+ as a minor constituent [89]. Surprisingly, significant intensities of energetic alpha particles from the solar wind were not observed at Uranus, as were seen by Voyager 2 at every other Giant planet [e.g. 90]. The primary source of protons is likely from ionization of Uranus' extended neutral hydrogen corona while the ionosphere and solar wind may also contribute [e.g. 84,91], but only in the outer magnetosphere with the solar wind protons not making it into the inner magnetosphere [92].

The electrons at Uranus also contained a thermal and non-thermal component, with significant inbound/outbound asymmetries in their densities and temperatures [93]. Meanwhile, the measured energetic (> 22 keV to ~1.2 MeV) electrons were seen at much higher fluxes than the ions, especially in the electron radiation belts, which were observed to be surprisingly as intense as Earth's [89]. Of course, as previously discussed, these measurements are all taken at one epoch with a particular orientation of the solar wind flow, dipole axis, and rotation axis; at this epoch heavier water group ions may be rapidly swept out of the magnetosphere [92,94] and which might not be the case at other epochs.

At Neptune, the plasma was observed to contain a significant heavy ion population (inferred to be N^+) in addition to the light (H^+) population [95], both of which increased in density and temperature (based on anisotropic Maxwellian fits to the spectra) as Voyager 2 approached the planet [88]. Thermal escape of H, H_2, and N from the atmosphere of Triton is thought to be the source for these populations, forming a neutral torus in Neptune's magnetosphere that is subsequently ionised to form the H^+ and N^+ populations measured by Voyager 2 [96,42]. Models suggest that <4% of the escape from Triton is in an ionised state thus not restricting mass-loading to the direct vicinity of Triton [96]. It was suggested that this ionization of the Triton neutral

torus is the dominant source of magnetospheric plasma for the most of Neptune's middle and outer magnetosphere, with lifetimes for N^+ of several weeks [97,98]. While models like Cheng [97] suggest that a Triton torus (neutral and/or plasma) is a significant source, it is unclear how long-lived the torii would be given Triton's highly inclined orbit and the dynamic variability and reorientation of the Neptunian magnetosphere on diurnal and seasonal timescales. For example, it is unclear how regularly the torii would intersect with the cusp regions as the planet rapidly rotates. This feeds back to the broader question regarding the dominant plasma transport and loss mechanisms in Neptune's magnetosphere, namely how the system sheds the mass continually introduced by Triton [e.g. 99]. These findings were in contrast with what is expected from adiabatic transport and what was observed at Uranus. Neptune's ionosphere may also be a source for the observed H^+. The mass-resolved energetic (> 500 keV/nuc) ion distributions consisted of H^+, H_2^+ and $^4He^+$ with a ratio of 1300:1:0.1, which were interpreted as originating from Neptune's ionosphere [100,27].

Most of the electron spectra in Neptune's magnetosphere was consistent with a cold Maxwellian component with one or two hot Maxwellian components [101] with significant changes in the shape between the Voyager 2 instrumentation [102]. Triton's minimum orbital distance was observed to be a highly organizing factor in general for many aspects of the energetic particle distribution, with radiation belt particles confined inside ~ 8 R_N and distinctive pitch angle distributions for both ions and electrons beyond this distance were suggestive of having been shaped by Triton and its possible extended neutral torus [42].

The complex magnetospheric topologies and diurnal and seasonal dynamics of the ice giant magnetospheres give rise to many peculiarities that test our understanding of magnetospheric transport processes and dynamics. For example, the large tilts between the planets' rotational and magnetic axes allows for unique opportunities to test the influences of different transport processes that are largely coupled in other planetary magnetospheres in the solar system. In the case of Uranus, specifically, the co-rotation and convection electric fields can become roughly orthogonal in certain seasons [48,94], allowing for distinction between flows resulting from tail reconnection and those arising from centrifugally-driven interchange instabilities [103]. Furthermore, Voyager 2 did not observe a plasmasphere of co-rotating plasma at Uranus [94], suggesting that it may be an even purer example of a magnetosphere with convection exclusively driven by the solar wind than Earth. Voyager 2 did observe apparent substorm-like injection signatures [25] and plasmoids [26], providing further evidence for such solar wind-driving; however, quite curiously, given this apparent solar wind-driving, the Uranian magnetosphere was found to be largely devoid of solar wind alpha particles and heavier ions [89], perhaps related to shielding of the inner magnetosphere [49]. It must be emphasized, that the ion mass composition in the suprathermal energy range from 10s to several 100s of keV, and the charge-state composition at all energies, was largely unexplored by the Voyager 2 instrumentation. Conversely, no evidence of processes associated with reconnection in Neptune's magnetosphere was observed; this may suggest that global mass shedding may be achieved via a more viscous-like global interaction with the more distant solar wind [12]. The absence of magnetic trapping on closed field lines at Neptune was provided as evidence for the dominance of interchange instabilities as the dominant transport mechanism [47].

6. Radiation Belts

The radiation belts of Uranus and Neptune present unique data points amongst the magnetized planets of the solar system. For example, the Voyager 2 observations at Uranus [25] differed greatly from what would be expected given our observations and subsequent conclusions from elsewhere in the solar system. Current understanding of planetary radiation belts holds that the accumulation of robust radiation belts (i.e., trapped populations of high energy particles) requires a large reservoir of lower energy plasma from which to draw, very slow loss processes for the accelerated particles, and/or very efficient acceleration processes. However, this did not appear to be the case at Uranus, which possesses a vacuum magnetosphere [83] lacking a source of low-energy plasma and where the most intense whistler-mode hiss waves observed by Voyager 2 were found [104]. The latter, in particular, raises several questions as these waves often lead to losses, while chorus waves, which were also observed at lower intensities, would provide efficient acceleration to create high energy particles, but can also result in significant particle losses. Lacking an apparent seed population and evidence for a strong loss mechanism, one would guess that Uranus would have very weak radiation belts. However, Voyager 2 found Uranus' electron radiation belts to be as significant in intensity at 1 MeV energy as those of Earth and Jupiter [29] (Figure 3, right). Even more puzzling is that the proton radiation belts at Uranus are much weaker than the electron belts [28] and seem to be much more consistent with expectations (Figure 3, left).

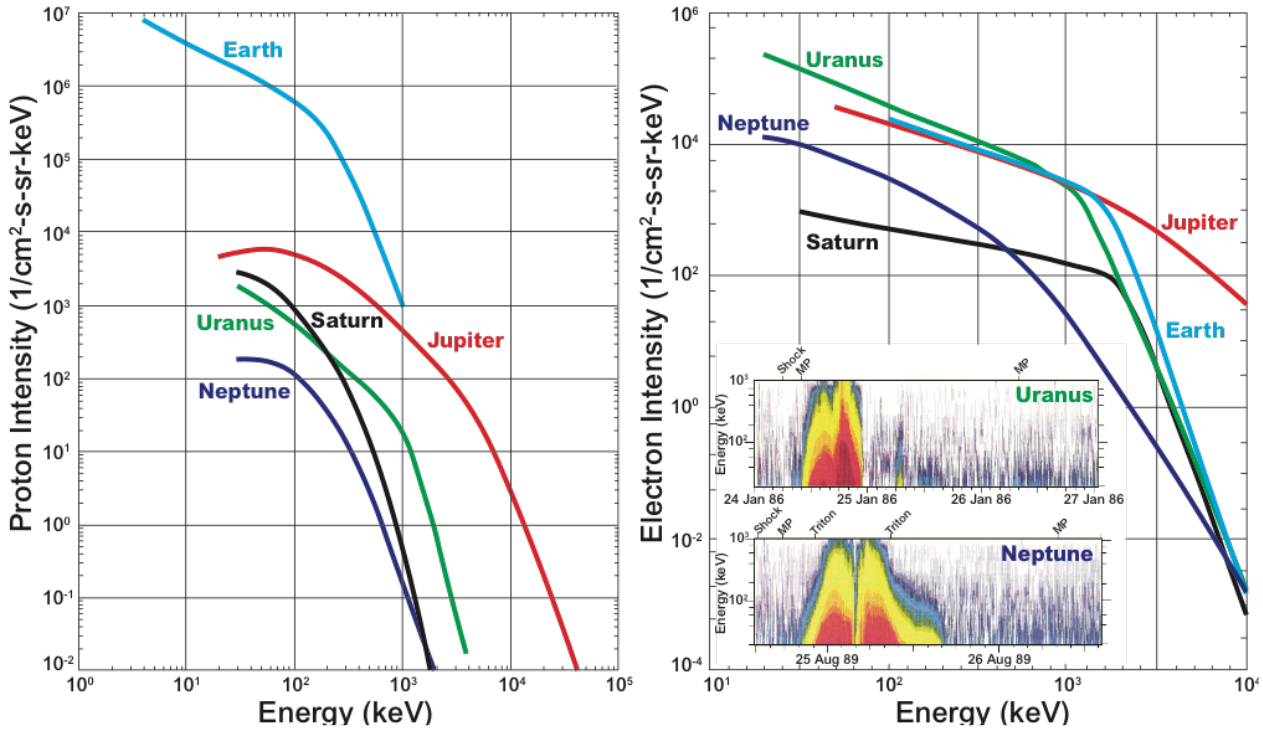

Figure 3: The most intense observed spectra of the proton (left; adapted from Mauk [28]) and electron (right; adapted from Mauk & Fox [29]) radiation belts of the ice giants compared to those found in other solar system magnetospheres. The inset shows the spectrograms of energetic electrons observed at Uranus and Neptune by Voyager 2 (from Mauk and Fox,[29]).

Conversely, Neptune's radiation environment was observed to be much more benign during the Voyager 2 encounter, with surprisingly weak ion radiation belts. This disparity could be attributable to fundamental differences between the global drivers of transport between the two planets – i.e., the possible absence of injections, which play a role at other planets, to transport and accelerate the low-energy plasma to the discussed high radiation energies at Neptune. It remains unclear whether these observed differences in radiation belts between the two ice giants could be due to Uranus' high obliquity and its effects on the magnetospheric processes at play, the influence of Triton at Neptune, the influence of interactions with yet-undiscovered rings, the local characteristics of the solar wind determining the type of interaction with the magnetosphere (which are linked to solar cycle and solar wind dynamics), and/or seasonal effects that happened to be prevalent during the Voyager 2 encounters. However, it is clear that these questions will not be addressable without long-term measurements from orbiter missions in both systems.

Both Uranus and Neptune have satellites with very dark surfaces [105], this is in stark contrast to the usually brighter satellites of gas giant planets. Lanzerotti et al. [106] suggested this might be due to surface weathering, with Thompson et al. [107] pointing out that darkening can result from energetic proton weathering if the surface composition includes methane. The ion composition of the ice giant radiation belts remains largely unknown after Voyager 2 and any further assessment on the origin of the ice giant satellite surface composition will await future orbital missions. See Kollmann et al. [108] and included references for additional discussion on this topic.

7. Aurora

The complex magnetic topology of the ice giants will influence the structure and location of the planets' auroral emissions, a fact that was exploited by Herbert [109] to improve models of Uranus' internal magnetic field. The auroral radio emissions from Uranus and Neptune were found to be unexpectedly rich with a range of emissions and structures not seen at other magnetized planets [e.g., 110, *Lamy*, this issue]. Our increasing catalog of remote auroral observations at Uranus with the Hubble Space Telescope [56,111] might enable us to improve these yet further and could eventually provide a way to probe how the Uranian magnetosphere evolves over time and influences heating of the atmosphere [112]. Voyager 2 observed very faint aurora on the dark side of Neptune [113], but no additional detections of auroral emissions at Neptune have been possible from Earth [114]. It is unclear how a potential auroral footprint from Triton might be manifest, given that the moon's orbit is highly inclined relative to the Neptune's rotational and magnetic axes, and the opportunity to make these observations *in situ* would doubtless provide a powerful tool in the complex magnetic mapping [97]. There are many unresolved questions regarding how these potentially complex auroral current systems would be configured or close given such dynamic magnetospheres [e.g., 115], and future magnetospheric and auroral observations at Uranus and Neptune could provide key insights into their form and function. For a comprehensive discussion of the current knowledge from ultraviolet, infrared, and radio emission observations, we direct the readers to the companion papers by *Melin et al.*, and *Lamy* in this issue.

8. Discussion

Complex geometries of the magnetospheres of Uranus and Neptune were advantageous for exploring much of the magnetospheres, enabling a single flyby of each planet to sample the bow shock, magnetopause, radiation belts, the plasma sheet, lobes, tail structure, and even the cusp/mantle. However insightful, the Voyager 2 encounters with these planets provided essentially a snapshot in time of these highly variable and asymmetric magnetospheres. It is impossible to know which of the observed phenomena were indicative of the system and which were manifestations of system dynamics - i.e., transient states that the systems happened to be in as the Voyager 2 spacecraft passed by - and it is this frustratingly absent diagnostic that drives most of the outstanding mysteries at these outermost solar system planets. This is a challenge for the interpretation of single spacecraft observations at any planet, but driven to extremes at Uranus and Neptune because there are no well-studied templates for these magnetospheres.

As it stands, we could be forgiven for thinking our solar system ice giants are very different from each other. Uranus was observed by Voyager 2 to have strong radiation belts and substorm-like injection phenomena, while Neptune was quiescent and displayed surprisingly weak radiation belts. However, modeling results summarized here demonstrate that this is likely a consequence of the seasonal tilt of the respective planet's magnetic axes during the Voyager 2 encounters. Uranus was in solstice configuration displaying a somewhat Earth-like configuration though rotating nearly about the Sun-Earth line with solar wind-driven convection reaching deep into the magnetosphere; Neptune was in a configuration that had its magnetic field pole-on to the solar wind once per ~16-hour rotation - perhaps allowing for more episodic 'emptying' of magnetospheric plasma. Without orbiting missions, it will be impossible to know for certain how enduring or ephemeral the magnetospheric features observed during the Voyager 2 encounters might be; however, indications from a growing number of modeling efforts of these complex systems suggest that seasonal transitions and diurnal effects at Uranus and Neptune may have strong impacts on the state of their magnetospheres.

One key intrinsic difference between the two magnetospheres is the presence of the planetary interloper, the dwarf planet (and likely Kuiper Belt object) Triton, in an inclined and retrograde orbit about Neptune. Unlike Neptune's remaining satellites, Triton has a young bright surface [116] as well as a robust exosphere [113,117] and evidence of plume activity [118], both of which provide significant neutrals and ions [42] to the magnetosphere. There was also the suggestion that Triton shapes Neptune’s radiation belts, with Voyager 2 seeing a transition in the radiation belt particles beyond Triton’s minimum orbital distance. How Triton extends its influence so dramatically inside the minimum L-shell it traverses remains a mystery.

Another fundamental difference may be nature of the magnetospheric interaction with the solar wind. With limited data from the outer solar system to characterize the solar wind properties and how they vary in time and with solar cycle, it is challenging to predict the coupling mechanism between the solar wind and magnetospheres of Uranus and Neptune. This alone may account for differences in their magnetospheric dynamics, whether they are driven by solar wind reconnection or a more viscous interaction, but requires observations over extended periods of time in the outer solar system.

One could discuss at length the necessity and broader impacts of magnetospheric observations and how they help to address important questions across the planetary community. The magnetospheric environment is host to and influences a range of planetary phenomena from the space weathering of satellites and the evolution of ocean worlds, to ring-magnetosphere-atmosphere interactions and dust transport, to the dynamics of planetary dynamos which indicate structure of ice giant interiors, to the role magnetic fields and charged particle precipitation might play in atmospheric heating. However, this broad discussion is well captured in Kollmann et al. [108]. As a review of ice giant magnetospheres, we present a restricted list of key questions raised by these outer solar system denizens:

- **How do the ice giant magnetospheres evolve dynamically?** What factors play a role in their similarities and differences? The orientation of the spin axis and dipole axis (e.g., both pole-on, both perpendicular, or a mix) form a set of limiting cases. Are these generally valid or are the ice giant magnetospheres almost never in these states?
- **What role does the solar wind play in driving magnetospheric dynamics and charged particle transport?** How prominent are the seasonal responses of these magnetospheres? Is there a solar cycle influence? How much external driving might be masked by drastic diurnal variations?
- **What role do moons (esp. Triton) and rings play in supplying the ice giant magnetospheres with plasma?** What are the proportions and source rates of neutrals and ions supplied to the ice giant magnetospheres? In the general case, the neutrals, plasma, and magnetic field are all on mutually-inclined (and probably non-planar) surfaces: How does this all change with season? What effect does this have on plasma sources, sinks, and circulation? What processes govern mass loss and mass balance? Is there an equilibrium state for either of the ice giant magnetospheres?
- **Why was Uranus observed to have such intense radiation belts and Neptune so benign at the time of Voyager 2's encounters?** What processes generate and sustain them? And are they fundamentally different, or similar but highly variable?
- **Can we remotely explore the ice giant magnetospheres via auroral observations from Earth orbiting telescopes** [see *Melin et al*. and *Lamy* in this issue]? Can observations of putative icy-moon auroral footpoints help to map their magnetic fields (as was done at Jupiter and Saturn)? How might the strongly seasonally modulated configuration of the ionosphere and the complex interior magnetic field influence magnetosphere-ionosphere coupling?

Following decades of exploration of all the other planetary magnetospheres in our solar system we have the instrumentation and expertise, in both modeling and data analysis, necessary to study these most complicated environments. Exploration of the magnetospheres of our solar system ice giants will challenge space scientists beyond anything we have encountered so far, but we are ready.

Additional Information

Data Accessibility
"This article has no data."

Authors' Contributions
Each co-author contributed significantly to the production of this manuscript. CP conceived the framework and content of the review, and contributed the majority of Section 1, and components of each section, CSA contributed the majority of Section 2 and created Figure 1, GAD contributed the majority of Sections 3 and 4, IJC and RWE contributed the majority of Section 5 and 6, IJC and AMR contributed the majority of Section 7, and AMR, CP, and CSA contributed the majority of Section 8. All authors read and approved the manuscript.

Competing Interests
The authors declare that they have no competing interests.

Funding Statement
Carol Paty gratefully acknowledges internal support from the University of Oregon. Chris Arridge is funded by a Royal Society Research Fellowship and a Science and Technology Facilities Council consolidated grant to Lancaster University. Gina DiBraccio gratefully acknowledges internal support from the Solar System Exploration Division within the NASA Goddard Space Flight Center (GSFC) Sciences and Exploration Directorate. Abigail Rymer and Ian Cohen were supported by internal funds from the APL Civil Space Mission Area. Rob Ebert is funded by Southwest Research Institute.

Acknowledgments
The authors would like to thank Dr. Chris Paranicas for his help and insights into the energetic particle discussion, and Dr. Barry Mauk and Dr. Peter Kollmann for conference talks and follow-up discussions that helped to inspire the talk on which this manuscript was based. CP also acknowledges the help of Joe Caggiano and Angela Olsen in assembling the manuscript.

References

1. Connerney N. E. P. 1993. Magnetic fields of the outer planets. *J. Geophys. Res.* **98**, E10, 659–679. (doi:10.1029/93JE00980)
2. Masters A. 2014. Magnetic reconnection at Uranus' magnetopause. *J. Geophys. Res.: Space Physics*, **119**, 7, 5520-5538. (doi:10.1002/2014JA020077)
3. Masters A. 2015. Magnetic reconnection at Neptune's magnetopause. *J. Geophys. Res.: Space Physics*, **120**, 1, 479-493. (doi:10.1002/2014JA020744)
4. Mejnertsen L, Eastwood JP, Chittenden JP, Masters A. 2016. Global MHD simulations of Neptune's magnetosphere, *J. Geophys. Res.: Space Physics*, **121**, 8, 7497-7513, (doi:10.1002/2015JA022272)
5. Cao X, Paty C. 2017. Diurnal and seasonal variability of Uranus's magnetosphere, *J.Geophys. Res.: Space Physics*, **122**, 6, 6318-6331, (doi:10.1002/2017JA024063)
6. Gershman DJ, DiBraccio GA. Solar cycle dependence of solar wind coupling with giant planet magnetospheres. *Geophys. Res. Lett.* Under Review.

7. Ness NF, Acuña MH, Behannon KW, Burlaga LF, Connerney JEP, Lepping RP, Neubauer FM. 1986. Magnetic fields at Uranus. *Science*, **233**, 4759, 85–89. (doi:10.1126/science.233.4759.85)
8. Behannon KW, Lepping RP, Sittler EC Jr., Ness NF, Mauk BH, Krimigis SM, McNutt RM Jr. 1987. The magnetotail of Uranus, *J. Geophys. Res.: Space Physics*, **92**, A13, 15354-15366. (doi:10.1029/JA092iA13p15354)
9. Hammond CM, Walker RJ, Kivelson MG. 1990. A Pincer-shaped plasma sheet at Uranus, *J. Geophys. Res.: Space Physics*, **95**, A9, 14987-14994, (doi:10.1029/JA095iA09p14987)
10. Toth G, Kovacs D, Hansen KC, Gombosi TI. 2004. Three-dimensional MHD simulations of the magnetosphere of Uranus, *J. Geophys Res: Space Physics*, **109**, A11, (doi:10.1029/2004JA010406)
11. Griton L, Pantellini F, Meliani Z. 2018. Three-Dimensional Magnetohydrodynamic Simulations of the Solar Wind Interaction With a Hyperfast-Rotating Uranus. *J. Geophys. Res.: Space Physics*, **123**, 7, 5394-5406. (doi:10.1029/2018JA025331)
12. Masters A. 2018. A more viscous-like solar wind interaction with all the giant planets, *Geophys. Res. Lett.*, **45**, 15, 7320-7329, (doi:10.1029/2018GL078416).
13. Richardson et al. 1995. The plasma environment of Neptune, in Neptune (Cruikshank, ed.), pp. 279–340. Univ. of Arizona, Tucson.
14. Borovsky JE, Valdivia JA. 2018. The Earth's Magnetosphere: A Systems Science Overview and Assessment. *Surv. Geophys.* **39**, 817–859. (doi:10.1007/s10712-018-9487-x)
15. Bagenal F, McKinnon WB, Dowling TE. 2004. Jupiter: The Planet, Satellites and Magnetosphere, Cambridge University Press, Cambridge, UK.
16. Dougherty MK, Esposito M, Krimigis S. 2009. Saturn from Cassini-Huygens. Springer, Netherlands. (doi:10.1007/978-1-4020-9217-6)
17. Bolton SJ, Thorne RM, Gurnett DA, Kurth WS, Williams DJ. 1997. Enhanced whistler-mode emissions: Signatures of interchange motion on the Io torus. *Geophys. Res. Lett.* **24**, 17, 2123-2126. (doi:10.1029/97GL02020)
18. Thorne RM, Armstrong,TP, Stone S, Williams DJ, McEntire RW, Bolton SJ, Gurnett DA, Kivelson MG. 1997. Galileo evidence for rapid interchange transport in the Io torus. *Geophys. Res. Lett.* **24**, 17, 2131-2134. (doi:10.1029/97GL01788)
19. Mauk BH, Mitchell DG, McEntire RW, Paranicas CP, Roelof EC, Williams DJ, Krimigis SM, Lagg A. 2004. Energetic ion characteristics and neutral gas interactions in Jupiter's magnetosphere, *J. Geophys Res.: Space Physics,* **109**, A9. (doi:10.1029/2003JA010270)
20. Hill TW, Rymer AM, Burch JL, Crary FJ, Young DT, Thomsen MF, Delapp D, André N, Coates AJ, Lewis GR. 2005. Evidence for rotationally driven plasma transport in Saturn's magnetosphere, *Geophys. Res. Lett.* **32**, 14. (doi:10.1029/2005GL022620)
21. Mauk BH, Saur J, Mitchell DG, Roelof EC, Brandt PC, Armstrong TP, Hamilton DC, Krimigis SM, Krupp N, Livi SA, Manweiler JW. 2005. Energetic particle injections in Saturn's magnetosphere, *Geophys. Res. Lett.* **32**, 14. (doi:10.1029/2006GL028676)

22. Burch JL, Goldstein J, Hill TW, Young DT, Crary FJ, Coates AJ, André N, Kurth WS, Sittler EC. 2005. Properties of local plasma injections in Saturn's magnetosphere, *Geophys. Res. Lett.* **32** 14. (doi:10.1029/2005GL022611)
23. Yung YL, Lyons JR. 1990. Triton: Topside ionosphere and nitrogen escape, *Geophys Res. Lett.* **17,** 10, 1717-20. (doi:10.1029/GL017i010p01717)
24. Mauk BH, Krimigis SM, Cheng AF. 1995 Energetic particles and hot plasmas of Neptune, in *Neptune and Triton.* Ed. Cruikshank DP. University of Ariona Press. 169-232.
25. Mauk BH, Krimigis SM, Keath EP, Cheng AF, Armstrong TP, Lanzerotti LJ, Gloeckler, G, Hamilton, DC. 1987. The hot plasma and radiation environment of the Uranian magnetosphere. *J. Geophys. Res. Space Physics*, **92**, A13, 15283-15308. (doi:10.1029/JA092iA13p15283)
26. DiBraccio GA, Gershman DJ. 2019. Voyager 2 constraints on plasmoid based transport at Uranus. *Geophys. Res. Lett.* **46**, 19, 10710-10718. (doi:10.1029/2019GL083909)
27. Mauk BH, Keath EP, Kane M, Krimigis SM, Cheng AF, Acuna MH, Armstrong TP, Ness NF. 1991. The magnetosphere of Neptune: Hot plasmas and energetic particles. *J. Geophys. Res. Space Physics*, **96**, S01, 19061-19084. (doi:10.1029/91JA01820)
28. Mauk BH. 2014. Comparative investigation of the energetic ion spectra comprising the magnetospheric ring currents of the solar system, *J. Geophys. Res.: Space Physics*, **119**, 9729–9746, (doi:10.1002/2014JA020392)
29. Mauk BH, Fox NH. 2010. Electron radiation belts of the solar system, *J. Geophys. Res.* **115**, A12220. (doi:10.1029/2010JA015660)
30. Jurac S, Johnson RE, Richardson JD. 2001. Saturn's E ring and production of the neutral torus. *Icarus* **149**, 2, 384-96. (doi:10.1006/icar.2000.6528)
31. Jurac S, Richardson JD. 2005. A self-consistent model of plasma and neutrals at Saturn: Neutral cloud morphology. *J. Geophys. Res.: Space Physics* **110**, A9. (doi:10.1029/2004JA010635)
32. Paranicas C, Mitchell DG, Krimigis SM, Hamilton DC, Roussos E, Krupp N, Jones GH, Johnson RE, Cooper JF, Armstrong TP. 2008. Sources and losses of energetic protons in Saturn's magnetosphere. *Icarus* **197**, 2, 516–525. (doi: 10.1016/j.icarus.2008.05.011)
33. Clark, G, C Paranicas, D Santos-Costa, S Livi, N Krupp, DG Mitchell, E Roussos, and W-L Tseng. 2014. Evolution of electron pitch angle distributions across Saturn's middle magnetospheric region from MIMI/LEMMS. *Planet. Space Sci.*, **104**, 18–28, (doi:10.1016/j.pss.2014.07.004)
34. Glatzmeier GA, Roberts PH. 1995. A three-dimensional self-consistent computer simulation of a geomagnetic field reversal. *Nature* **377**. 203-209. (doi:10.1038/377203a0)
35. Lepping RP. 1994. Comparisons of the field configurations of the magnetotails of Uranus and Neptune. *Planetary and Space Science* **42**, 10, 847–857. (doi:10.1016/0032-0633(94)90065-5)
36. Arridge CS, Paty C, Giant Planets – Asymmetrical Magnetospheres: Uranus and Neptune, Chapter 8.5 in Magnetospheres, ed. Maggiolo R, André N, Hasegawa H, Welling D. AGU Books, Wiley. (In Press)
37. Ness NF, Acuña MH, Burlaga LF, Connerney JEP, Lepping RP, Neubauer FM. 1989. Magnetic fields at Neptune. *Science* **246**, 4936, 1473–1478. (doi:10.1126/science.246.4936.1473)

38. Uno H, Johnson CL, Anderson BJ, Korth H, Solomon SC. 2009. Modeling Mercury's internal magnetic field with smooth inversions. *Earth and Planetary Science Lett.* **285**, 3-4, 328-339. (doi:10.1016/j.epsl.2009.02.032)
39. Anderson BJ, Johnson CL, Korth H, Purucker ME, Winslow RM, Slavin JA, Solomon SC, McNutt RL, Raines JM, Zurbuchen TH. 2011. The Global Magnetic Field of Mercury from MESSENGER Orbital Observations. *Science* **333**, 6051, 1859-1862. (doi: 10.1126/science.1211001)
40. Arridge CS. 2015. Magnetotails of Uranus and Neptune. Magnetotails in the Solar System,119–133. Wiley. Hoboken, NJ. doi:10.1002/9781118842324.ch7.
41. Cummings WD, Dessler AJ, Hill TW. 1980. Latitudinal oscillations of plasma within the Io torus. *J. Geophys. Res.* **85**, A5, 2108. (doi:10.1029/JA085iA05p02108)
42. Decker RB, Cheng AF. 1994. A model of Triton's role in Neptune's magnetosphere. *J. Geophys. Res.* **99**, E9, 19027. (doi:10.1029/94JE01867)
43. Arridge CS, Wiggs, J. 2019. Ikuchi: 3D Views of Solar System Magnetospheres. Zenodo (doi:10.5281/zenodo.3451443)
44. Lowes FJ. 1994. The geomagnetic eccentric dipole: facts and fallacies. *Geophys. J. Intl.*, **118**, 3, 671–679. (doi:10.1111/j.1365-246X.1994.tb03992.x)
45. Stanley S, Bloxham J. 2006. Numerical dynamo models of Uranus' and Neptune's magnetic fields. *Icarus* **184**, 2, 556-572. (doi:10.1016/j.icarus.2006.05.005)
46. McIlwain, C. E. 1961. Coordinates for mapping the distribution of magnetically trapped particles, *J. Geophys. Res.*, **66**(11), 3681– 3691, (doi:10.1029/JZ066i011p03681)
47. Paranicas C, Cheng AF. 1993. Absence of magnetic trapping on closed field lines at Neptune. *Geophys. Res. Lett.*, **20**, 24, 2805–2808. (doi:10.1029/93GL02430)
48. Vasyliunas VM. 1986. The convection-dominated magnetosphere of Uranus. *Geophys. Res. Lett.* **13**, 7, 621–623. (doi:10.1029/GL013i007p00621)
49. Selesnick RS. 1988. Magnetospheric convection in the nondipolar magnetic field of Uranus. *J. Geophys. Res. 93,* A9, 9607. (doi:10.1029/ja093ia09p09607)
50. Bagenal F. 1992. Giant Planet Magnetospheres. *Annual Review of Earth and Planetary Sciences*, **20**, 1, 289–328. (doi:10.1146/annurev.earth.20.1.289)
51. Cairns IH., Smith CW, Kurth WS, Gurnett DA, Moses S. 1991. Remote Sensing of Neptune's Bow Shock: Evidence for Large-Scale Shock Motions, *J. Geophys. Res.* **96**, 153-19,169
52. Szabo A, Siscoe GL, Lazarus AJ, McNutt RL, Lepping RP, Ness NF. 1991. Magnetopause and cusp observations at Neptune. *J. Geophys. Res.* **96**, S01, 19149. (doi:10.1029/91ja01600)
53. Siscoe GL. 1975. Particle and field environment of Uranus. *Icarus* **24**, 311-324.
54. Hill TW, Dessler AJ, Rassbach ME. 1983. Aurora on Uranus: A Faraday disc dynamo mechanism. *Planetary and Space Science* **31**, 10, 1187-1198. (doi: 10.1016/0032-0633(83)90110-1)
55. Cowley, S. W. H. 2013. Response of Uranus' auroras to solar wind compressions at equinox, *J. Geophys. Res. Space Physics*, **118**, 2897–2902, (doi:10.1002/jgra.50323)
56. Lamy L, et al. 2012. Earth-based detection of Uranus' aurorae. *Geophys. Res. Lett.* **39**, 7. (doi:10.1029/2012GL051312)

57. Voigt GH, Behannon KW, Ness NF. 1987. Magnetic field and current structures in the magnetosphere of Uranus. *J. Geophys. Res.: Space Physics* **92**, A13, 15337-15346. (doi:10.1029/JA092iA13p15337)
58. Voigt GH, Ness NF. 1990. The magnetosphere of Neptune: Its response to daily rotation. *Geophys. Res. Lett.* **17**, 10, 1705-1708. (doi:10.1029/GL017i010p01705)
59. Jackman CM, Slavin JA, Cowley SWH. 2011. Cassini observations of plasmoid structure and dynamics: Implications for the role of magnetic reconnection in magnetospheric circulation at Saturn. *J. Geophys. Res.* **116**, A10212 (doi:10.1029/2011JA016682)
60. Jackman CM, Slavin JA, Kivelson MG, Southwood DJ, Achilleos N, Thomsen MF, et al. 2014. Saturn's dynamic magnetotail:A comprehensive magnetic field and plasma survey of plasmoids and traveling compression regions and their role in global magnetospheric dynamics. *J. Geophys. Res.: Space Physics*, **119**, 5465–5494. doi: 10.1002/2013JA019388
61. Vogt MF, Jackman CM, Slavin JA, Bunce EJ, Cowley SWH, Kivelson MG, Khurana KK. 2014. Structure and statistical properties of plasmoids in Jupiter's magnetotail. *J. Geophys. Res.: Space Physics*, **119**, 821–843. (doi:10.1002/2013JA019393)
62. Vogt MF, Connerney JEP, DiBraccio GA, Wilson RJ, Thomsen MF, Ebert RW, et al. 2020. Magnetotail reconnection at Jupiter: A survey of Juno magnetic field observations. *J. Geophys. Res.: Space Physics*, **125**, e2019JA027486. (doi:10.1029/2019JA027486)
63. Richardson IG, Cowley SWH, Hones EW, Bame SJ. 1987. Plasmoid-associated energetic ion bursts in the deep geomagnetic tail: Properties of plasmoids and the postplasmoid plasma sheet. *J. Geophys. Res.* **92**, 9,997–10,013. (doi:10.1029/JA092iA09p09997)
64. Richardson JD, Belcher JW, Selesnick RS, Zhang M, Siscoe GL, Eviatar A. 1988. Evidence for periodic reconnection at Uranus? *Geophys. Res. Lett.* **15**, 8, 733–736. (doi: 10.1029/GL015i008p00733)
65. Parker E. N. 1958, Dynamics of the interplanetary gas and magnetic fields, Astrophys. J., 128, 664, (doi:10.1086/146579)
66. Swisdak M, Rogers BN, Drake JF, Shay MA. 2003. Diamagnetic suppression of component magnetic reconnection at the magnetopause, *J. Geophys. Res.* **108**, A5, 1218, (doi:10.1029/2002JA009726)
67. Swisdak M, Opher M, Drake JF, Bibi FA. 2010. The vector direction of the interstellar magnetic field outside the heliosphere, Astrophys. J. 710, 1769–1775, doi:10.1088/0004-637X/710/2/1769.
68. DiBraccio GA, Slavin JA, Boardsen SA, Anderson BJ, Korth H, Zurbuchen TH, Raines JM, Baker DN, McNutt RL, Solomon SC. 2013. MESSENGER observations of magnetopause structure and dynamics at Mercury. *J. Geophys. Res.: Space Physics* **118**, 3, 997-1008. (doi:10.1002/jgra.50123)
69. Gershman DJ, Slavin JA, Raines JM, Zurbuchen TH, Anderson BJ, Korth H, Baker DN, Solomon SC. 2013. Magnetic flux pileup and plasma depletion in Mercury's subsolar magnetosheath. *J. Geophys. Res.: Space Physics* **118**, 11, 7181-7199. (doi:10.1002/2013JA019244)
70. Phan TD, Paschmann G, Gosling JT, Oieroset M, Fujimoto M, Drake JF, Angelopoulos V. 2013. The dependence of magnetic reconnection on plasma beta and magnetic shear: evidence from magnetopause observations. *Geophys. Res. Lett.* **40,** 1, 11–16. (doi:10.1029/2012gl054528)

71. Fuselier SA, et al. 2017. Large-scale characteristics of reconnection diffusion regions and associated magnetopause crossings observed by MMS, J. Geophys. Res. Space Physics, 122, 5466–5486, (doi:10.1002/2017JA024024)
72. Desroche M, Bagenal F, Delamere PA, Erkaev N. 2012. Conditions at the expanded Jovian magnetopause and implications for the solar wind interaction, *J. Geophys. Res.* **117**, A07202, (doi:10.1029/2012JA017621)
73. Ebert RW, et al. 2017, Accelerated flows at Jupiter's magnetopause: Evidence for magnetic reconnection along the dawn flank, *Geophys. Res. Lett.* **44**, 4401–4409, (doi:10.1002/2016GL072187)
74. Masters A. 2017. Model-based assessments of magnetic reconnection and Kelvin-Helmholtz instability at Jupiter's magnetopause. *J. Geophys. Res.: Space Physics*, **122**, 11154–11174. (doi:10.1002/ 2017JA024736)
75. Desroche M, Bagenal F, Delamere PA, Erkaev N. 2013. Conditions at the magnetopause of Saturn and implications for the solar wind interaction. *J. Geophys. Res. Space Physics* **118**, 3087– 3095, (doi:10.1002/jgra.50294)
76. Masters A, Eastwood JP, Swisdak M, Thomsen MF, Russell CT, Sergis N, Crary FJ, Dougherty MK, Coates AJ, Krimigis SM. 2012, The importance of plasma β conditions for magnetic reconnection at Saturn's magnetopause, *Geophys. Res. Lett.* **39**, L08103. (doi:10.1029/2012GL051372)
77. Bagenal, F., Delamere, P. A., Elliott, H. A., Hill, M. E., Lisse, C. M., McComas, D. J., McNutt Jr, R. L., Richardson, J. D., Smith, C. W., & Strobel, D. F. 2015. Solar wind at 33 AU: Setting bounds on the Pluto interaction for New Horizons. *Journal of Geophysical Research: Planets*, **120**, 1497– 1511.(doi:10.1002/2015JE004880)
78. Bagenal F, Belcher JW, Sittler EC, Lepping RP. 1987. The Uranian bow shock: Voyager 2 inbound observations of a high Mach number shock, *J. Geophys. Res.* **92**, A8, 8603– 8612, (doi:10.1029/JA092iA08p08603)
79. Szabo A, Lepping RP. 1995. Neptune inbound bow shock. *J. Geophys. Res.: Space Physics* **100**, A2, 1723-1730. (doi:10.1029/94JA02491)
80. Bridge HS, Belcher JW, Butler RJ, Lazarus AJ, Mavretic AM, Sullivan JD, Siscoe GL, Vasyliunas VM. 1977. The Plasma Experiment on the 1977 Voyager Mission. *Space. Science. Rev.* **21**, 3, 259-287. (doi:10.1007/BF00211542).
81. Krimigis SM, Armstrong TP, Axford WI, Bostrom CO, Fan CY, Gloeckler G, Lanzerotti LJ. 1977. The Low Energy Charged Particle (LECP) experiment on the Voyager spacecraft. *Space Science Rev.* **21**, 329-354.
82. Bridge HS, et al. 1986. Plasma Observations Near Uranus: Initial Results from Voyager 2. *Science* **233**, 4759, 89-93. (doi:10.1126/science.233.4759.89).
83. McNutt RL Jr., Selesnick RS, Richardson JD. 1987. Low-energy plasma observations in the magnetosphere of Uranus. *J. Geophys. Res.: Space Physics* **92**, A5, 4399-4410. (doi:10.1029/JA092iA05p04399)
84. Selesnick RS, McNutt RL Jr. 1997. Voyager 2 plasma ion observations in the magnetosphere of Uranus. *J. Geophys. Res.: Space Physics - Voyager 2 at Uranus.* 15249-15262. doi:10.1029/JA092iA13p15249.
85. Bagenal F, Delamere PA. 2011. Flow of mass and energy in the magnetospheres of Jupiter and Saturn. *J. Geophys. Res.: Atmospheres* **116**, A5, 5209. (doi: 10.1029/2010JA016294)
86. Pontius D, Hill TW. 2009. Inertial corotation lag and mass loading in Saturn's magnetosphere, *Geophys. Res. Lett.* **36**, L23103, (doi:10.10292009GL041030)

87. Chen Y, Hill TW, Rymer AM, Wilson RJ. 2010. Rate of radial transport of plasma in Saturn's inner magnetosphere, *J. Geophys. Res.* **115**, A10211, (doi:10.1029/2010JA015412)
88. Richardson JD, et al. 1991, Low-energy ions near Neptune, *J. Geophys. Res.* **96**, 18993 – 19011. (doi:10.1029/91JA01598)
89. Krimigis SM, Armstrong TP, Axford WI, Cheng AF, Gloeckler DC, Hamilton DC, Keath EP, Lanzerotti LJ, Mauk BH. 1986. The Magnetosphere of Uranus: Hot Plasma and Radiation Environment. *Science* **233**, 4759, 97-102. (doi:10.1126/science.233.4759.97)
90. Cheng A.F. (1997) Magnetospheres of the outer planets. In: Encyclopedia of Planetary Science. Encyclopedia of Earth Science. Springer, Dordrecht. (doi:10.1007/1-4020-4520-4_231)
91. Belcher JW, McNutt RL Jr., Richardson JD, Selesnick RS, Sittler EC Jr., Bagenal F. 1991. The plasma environment of Uranus, in *Uranus*.University of Arizona Press, Tucson, AZ. 780-830.
92. Cheng, A. F. 1987. Proton and oxygen plasmas as Uranus, *J. Geophys. Res.*, **92**(A13), 15,309–15,314. (doi:10.1029/JA092iA13p15309)
93. Sittler EC, Ogilvie KW, Selesnick R. 1987. Survey of electrons in the Uranian magnetosphere: Voyager 2 observations. *J. Geophys. Res.: Space Physics* **92**, A13, 15263-15281. (doi:10.1029/JA092iA13p15263)
94. Selesnick RS, Richardson JD. 1986. Plasmasphere formation in arbitrarily oriented magnetospheres. Geophys. Res. Lett. **13**, 7, 624-627. (doi:10.1029/GL013i007p00624)
95. Belcher JW et al. 1989. Plasma Observations Near Neptune: Initial Results from Voyager 2. *Science* **246**, 4936, 1478-1483. (doi:10.1126/science.246.4936.1478)
96. Summers, M. E., and D. F. Strobel. 1991. Triton's atmosphere: A source of N and H for Neptune's magnetosphere, *Geophys. Res. Lett.*, **18**, 2309-2312 (doi: 10.1029/91GL01334)
97. Cheng AF. 1990. Global Magnetic Anomaly and Aurora of Neptune. *Geophys. Res. Lett.* **17**, 10, 1697-1700. (doi:10.1029/GL017i010p01689)
98. Cheng AF, Maclennan CG, Mauk BH, Krimigis SM, Lanzerotti LJ. 1992. Energetic ion phase space densities in Neptune's magnetosphere. *Icarus*. **99**, 2, 420-429. (doi:10.1016/0019-1035(92)90157-3)
99. Richardson JD. 1993. A quantitative model of plasma in Neptune's magnetosphere. *Geophys. Res. Lett.* **20**, 14, 1467-1470. (doi:10.1029/93GL01353)
100. Krimigis SM, et al. 1989. Hot plasma and energetic particles in Neptune's magnetosphere, Science, 246, 1483. (doi:10.1126/science.246.4936.1483)
101. Zhang, M., Richardson, J. D., and Sittler, E. C. 1991. Voyager 2 electron observations in the magnetosphere of Neptune. *J. Geophys. Res.*, **96**(S01), 19085– 19100, (doi:10.1029/91JA01857)
102. Sittler, E. C., and Hartle, R. E. (1996), Triton's ionospheric source: Electron precipitation or photoionization, *J. Geophys. Res.*, **101**(A5), 10863– 10876, (doi:10.1029/96JA00398)
103. Mitchell, DG, et al. 2015. Injection, interchange, and reconnection, In *Magnetotails in the Solar System*, AGU Geophysical Monograph Series, A. Kelling, C. M. Jackman, and P. Delamare (Eds.), (doi:10.1002/9781118842324.ch19)
104. Kurth WS, Gurnett DA. 1991. Plasma waves in planetary magnetospheres. *J. Geophys. Res.: Space Physics* **96**, S01, 18977-18991. (doi:10.1029/91JA01819)
105. Karkoschka, E. 2001. Comprehensive Photometry of the Rings and 16 Satellites of Uranus with the Hubble Space Telescope. *Icarus*. **151** (1): 51–68. (doi:10.1006/icar.2001.6596)

106. Lanzerotti LJ, Brown WL, Maclennan CG, Cheng AF, Krimigis SM, Johnson RE. 1987. Effects of charged particles on the surfaces of the satellites of Uranus. *J. Geophys. Res.* **92**(A13), 14949–14957. (doi.org/10.1029/JA092iA13p14949)
107. Thompson WR, Murray BGJPT, Khare BN, Sagan C. 1987. Coloration and darkening of methane clathrate and other ices by charged particle irradiation: Applications to the outer solar system. *J. Geophys. Res.: Space Physics.* **92**, A13, 14933-14947. (doi:10.1029/JA092iA13p14933)
108. Kollmann P, et al. 2020. Magnetospheric Studies: A Requirement for Addressing Interdisciplinary Mysteries in the Ice Giant Systems. *Space Science Rev.* **216**, 78. (doi:10.1007/s11214-020-00696-5)
109. Herbert F. 2009. Aurora and magnetic field of Uranus. *J. Geophys. Res.: Space Physics* **114**, A11. (doi:10.1029/2009JA014394)
110. Zarka P. 1998. Auroral radio emissions at the outer planets: observations and theories. *J. Geophys. Res.* **103**, E9, 20159-20194. (doi:10.1029/98JE01323)
111. Lamy L, et al. 2017. The aurorae of Uranus past equinox. *J. Geophys. Res.: Space Physics* **122**, 4, 3997-4008. (doi:10.1002/2017JA023918)
112. Melin H, Fletcher LN, Stallard TS, Miller S, Trafton LM, Moore L, O'Donoghue J, Vervack RJ, Dello Russo N, Lamy L, Tao C, Chowdhury MN. 2019. The H3+ ionosphere of Uranus: decades-long cooling and local-time morphology. *Phil. Trans. R. Soc. A.* **377**, 2154. (doi:10.1098/rsta.2018.0408)
113. Broadfoot AL, et al. 1989. Ultraviolet Spectrometer Observations of Neptune and Triton. *Science* **246**, 4936, 1459-1466. (doi:10.1126/science.246.4936.1459)
114. Melin H, Fletcher LN, Stallard TS, Johnson RE, O'Donoghue J, Moore L, Donnelly PT. 2017. The quest for H3+ at Neptune: deep burn observations with NASA IRTF iSHELL. *Mon. Not. of the R. Astron. Soc.* **474**, 3, 3714-3719. (doi:10.1093/mnras/stx3029)
115. Mauk B, Bagenal F. 2012. Comparitive Auroral Physics: Earth and Other Planets. *Auroral Phenomenology and Magnetospheric Processes: Earth And Other Planets* **197**. (doi:10.1029/2011GM001192)
116. Smith BA et al. 1989. Voyager 2 at Neptune: Imaging Science Results. *Science* **246**, 4396, 1422-1449. (doi: 10.1126/science.246.4936.1422)
117. Tyler GL, et al. 1989. Voyager Radio Science Observations of Neptune and Triton. *Science* **246**, 4936, 1466-1473. (doi:10.1126/science.246.4936.1466)
118. Soderblom LA, Kieffer SW, Becker TL, Brown RH, Cook AF II, Hansen CJ, Johnson TV, Kirk RL, Shoemaker EM. 1990. Triton's Geyser-Like Plumes: Discovery and Basic Characterization. *Science* **250**, 4979, 410-415. (doi:10.1126/science.250.4979.410)

Figure and table captions

Figure 1: Sketch of the offset tilted dipole field lines (red), dipole axis $\boldsymbol{M}$ *(red), rotation axis* $\boldsymbol{\Omega}$ *(black) for Uranus (left) and Neptune (right). Note that the north and south poles are reversed in this view for the left panel as we draw this schematic using the IAU definition for Uranus' poles. The white lines mapped over the planets illustrate the rotational axis and rotational equator, and the red dashed line is the magnetic axis,*

hashed at the off-centered location of the magnetic moment. The ring plane is identified by the schematic representation of the discrete and diffuse rings in black.

Figure 2: Uranus' magnetotail as observed by Voyager 2's outbound trajectory where it (a) passed through the alternating polarity of the lobes (from Figure 5 in Ness et al., [7]). Panel (b) shows the inferred curved plasma sheet geometry (from Figure 5, Behannon et al. [8]), and panel (c) the model prediction of the twisted helical tail (after Toth et al. [10] and Arridge, [39]). Panel (d) shows the modelled rotation of the curved plasma sheet in a slice looking down-tail during Uranus solstice conditions (from Cao and Paty [5]). The last panel (e) is a visualization of the modelled current sheet of Neptune looking down-tail for the pole-on configuration (from Mejnertsen et a. [4]).

Figure 3: The most intense observed spectra of the proton (left; adapted from Mauk [28]) and electron (right; adapted from Mauk & Fox [29]) radiation belts of the ice giants compared to those found in other solar system magnetospheres. The inset shows the spectrograms of energetic electrons observed at Uranus and Neptune by Voyager 2 (from Mauk and Fox,[29]).